Direct Numerical Simulation Modeling of Multidisciplinary Transport during Li-Ion Battery Charge/Discharge Processes

Fangming Jiang*, Jianbang Zeng, Peng Peng and Shaoyang He

Laboratory of Advanced Energy Systems, CAS Key Laboratory of Renewable Energy, Guangzhou Institute of Energy Conversion, Chinese Academy of Sciences (CAS), Guangzhou 510640, China

Abstract: We develop a direct numerical simulation (DNS) model of multidisciplinary transport coupled with electrochemical reactions during Li-ion battery charge/discharge processes based on the finite volume (FV) numerical technique. Different from macroscopic models, the DNS model is based on microstructure of composite electrodes and solves component-wise transport equations. During DNS, the input physical properties are intrinsic material properties, not effective physical properties for macroscopic models. Since the interface of solid and electrolyte phase is evidently differentiated in DNS, the occurrence of electrochemical reactions is prescribed exactly on the interface of solid and electrolyte phase. Therefore, the DNS model has the potential to unravel the underlying mesoscopic pore-scale mechanisms of multi-disciplinary transport coupled with electrochemical reactions and thus can provide insightful information of the involved processes, as well as enables the design and optimization of electrodes, including microstructures inside electrodes. One test case, in which the electrode microstructure is reconstructed with a purely random reconstruction method, is considered. Simulation results corroborate the validity of the DNS model.

Keywords: Lithium-ion battery, Pore-scale model, Direct numerical simulation, Multidisciplinary transport.

1. INTRODUCTION

Lithium-ion batteries, since first commercialized by Sony in 1990s, have been widely used as power sources for mobile and stationary consumer electronics, and are perceived to be promising alternatives to power sources of electric vehicles and other medium- to large-sized power or energy storage devices, owing to relatively high energy and power densities, zero or low memory effect, and low self-discharge, etc. However, some fundamental mechanisms of lithium-ion battery processes still remain unknown or have not yet reached a widely-accepted cognition. Safety issues, poor cycle life, and high cost etc. continually remind us that the related technologies are still far away from a perfect state. [1,2]

While experiments are necessary to study the underlying physical chemistry of materials used in lithium-ion batteries and evaluate the battery performance, computational models are useful in providing a fundamental understanding of internal transport mechanisms, and are playing an increasingly important role in research, design and optimization of lithium-ion batteries. In the past two decades, various numerical models have been developed for lithium-ion batteries, such as, the isothermal electrochemical models by West *et al*. [3] and by Doyle *et al*. [4]. Thermal behaviors of lithium-ion battery affect its cycle life and safety operation. Pals and Newman [5,6] developed a one-dimensional thermal model for a single-cell lithium/polymer battery and later extended for a cell stack. Chen and Evans [7] developed a two-dimensional model, later extended to three-dimensional [8], to study the effects of various cell components, stack size and cooling conditions on the performance of Li-polymer electrolyte batteries under different discharge rates. Gu and Wang [9] and Srinivsan and Wang [10] developed a thermal-electrochemical coupled model for lithium-ion cells. Jiang *et al*. [11] presented an electrochemical-thermal coupled model and used it to explore thermal behaviors of a $LiFePO_4$ cell during discharge processes.

The above-summarized models can be generally classified as macroscopic models. The macroscopic electrochemical models solve simultaneously the charge (Li^+ in electrolyte phase and electron in solid phases) and species (Li^+ in electrolyte phase and Li in solid active materials) transport equations. The macroscopic thermal- electrochemical models are developed based on the electrochemical model coupled with an energy conservation equation, and has been validated to be useful in the research and development of lithium-ion batteries. [11] The macroscopic models provide some insight into the limiting mechanisms and predict behaviors of batteries under a wide range of operating conditions, thus a powerful tool for design and optimization of lithium-ion battery energy systems. However, the macroscopic models generally assume the electrodes and separator are homogenous porous media with all the detailed

*Address correspondence to this author at the Laboratory of Advanced Energy Systems, CAS Key Laboratory of Renewable Energy, Guangzhou Institute of Energy Conversion, Chinese Academy of Sciences (CAS), Guangzhou 510640, China; Tel: +86 20 87057656 ; Fax: +86 20 87057656;
E-mail: fm_jiang2000@yahoo.com

E-ISSN: 2409-5826/14

morphology about microscopic pore-structures neglected. That is to say, everywhere inside the electrodes and separator, the electrolyte and solid matrix coexist and the only characteristic parameter used to delineate the porous structure is the component fraction (or porosity). Physical properties are approximated in terms of the component fraction based on a concept of equivalence. This macroscopic treatment to the electrodes and separator of lithium-ion batteries may lose validity for real lithium-ion batteries due to its intrinsic defect of disregarding effects of electrode/separator microstructures. For better describing the cell behaviors and engineering the pore- or particle- scale microstructures of electrodes and separator, it is necessary to resort to mesoscopic pore-scale direct numerical simulations (DNS) [12].

The concept of DNS was originally from the modeling of flow turbulence in computational fluid dynamics, in which the Navier-Stokes equations were solved directly, without any turbulence models such as Reynolds averaging implemented, to resolve micro-level vortices [13,14]. The DNS approach has been used to study the correlation of performance and microstructure of proton exchange membrane fuel cell (PEMFC) electrodes [15-18]. In recent years, a few researchers attempted to do pore-scale DNS models of lithium-ion battery processes. Zhang *et al*. [19] considered a single particle and simulated intercalation- induced stresses and heat generation induced stresses inside $LiMn_2O_4$ particles. Wang and Sastry [20] developed a mesoscopic pore-scale model based on a microstructural system of regularly or randomly packing spherical or ellipsoidal particles, which represent the solid active materials in electrodes. Garcia *et al*. [21], Garcia and Chiang [22], and Smith *et al*. [23] proposed a pore-scale electrochemical model and used it to investigate the electrode microstructural effects and to design electrodes. To gain insight into the collector-electrode interactions, including mechanical deformation and contact resistance, Awarke *et al*. [24] established a three-dimensional mesoscopic particle-scale model, in which a representative volume element was generated using either a random packing or a dynamic collision algorithm considering different phases inside the electrodes. However, all the pre-mentioned DNS models for Li-ion batteries to some extent simplified the microstructures of electrodes, considered solely a stand-alone electrode or a half-cell at most, and commonly did not attempt to solve the involved multidisciplinary (e.g., electrochemical-thermal) coupling transport during charge/discharge processes.

The present work is aimed to develop a DNS model of multidisciplinary transport in Li-ion batteries during charge/discharge processes based on the finite volume (FV) numerical technique. To the best of our knowledge, this work is the first that attempts to do 3-dimensional DNS modeling of a full Li-ion cell. Microstructures of electrodes are reconstructed by a purely random reconstruction method. We will perform simulations to the discharge processes of Li-ion battery and analyze the simulation results to demonstrate the validity of the developed model.

2. DNS MODELING

2.1. Physicochemical Description

We take the $LiCoO_2|LiPF_6|LiC_6$ battery as an example. It consists of an anode current collector (Cu), an anode electrode, a separator, a cathode electrode, and a cathode current collector (Al), schematically shown in Figure **1**. The electrodes and separator are all composite. From FIB/SEM images, we can distinguish the components that make up the electrodes and separator. Three components are distinguished in the anode electrode: Li_xC_6 as active materials, pores full of electrolyte, and additives (CMC+SBR etc.). The three distinguishable phases in the cathode electrode are the active materials $Li_{y-x}CoO_2$, the electrolyte filling the pores, and additives (SP+PVDF etc.). The composite separator consists of polymer matrix and electrolyte. The electrolyte, a good ionic conductor but an electronic insulator, provides a medium for Li^+ to travel between the two electrodes and keeps electrons flowing in the solid phases (except polymer matrix) and along the external circuit. Electrochemical reactions occurring at the solid active materials/ electrolyte interfaces are as follows.

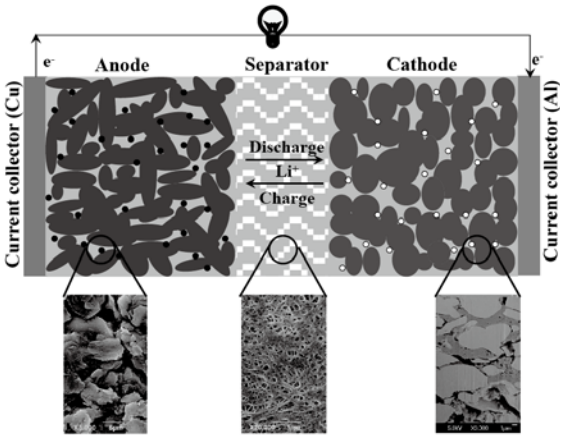

Figure 1: Schematic of a lithium-ion battery. On the second row are presented typical FIB/SEM images of electrodes and separator.

For the graphite electrode:

$$Li_xC_6 \underset{\text{charge}}{\overset{\text{discharge}}{\rightleftharpoons}} Li_0C_6 + xLi^+ + xe^- \quad (1)$$

For the $Li_{y-x}CoO_2$ electrode:

$$Li_{y-x}CoO_2 + xLi^+ + xe^- \underset{\text{charge}}{\overset{\text{discharge}}{\rightleftharpoons}} Li_yCoO_2 \quad (2)$$

During discharge, Li extracts from Li_xC_6 particles in the anode electrode (Eq. (1)), travels in the electrolyte, passes the separator and inserts into $Li_{y-x}CoO_2$ particles in the cathode electrode (Eq. (2)). Simultaneously, electrons released travel in the solid phases (including additives and active materials), flow through an external circuit into the cathode, and are then consumed by the cathode reaction. During charge the reverse processes occur.

2.2. Reconstruction of Electrodes

In the present work, we consider a purely random method for the reconstruction of electrodes. The cell is discretized to generate numerical elements and we then randomly specify some numerical elements as a certain component in terms of the component fraction. Figure **2** displays the component distributions and volume fractions in the computer-generated electrodes. The numerical elements are of dimensions 1×1×1 μm.

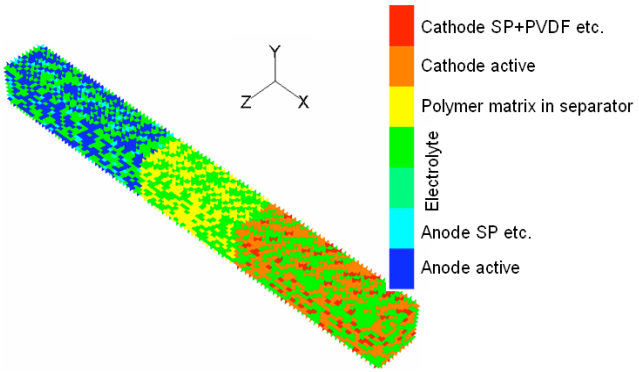

Anode (%)		
Li_xC_6	Electrolyte	SP etc.
45.1	45.5	9.4
Cathode (%)		
Li_yCoO_2	Electrolyte	SP+PVDF etc.
45.8	45.2	9.0
Separator (%)		
Polymer	Electrolyte	
53.4	46.6	

Figure 2: Component distributions and quantitative volume fractions in electrodes reconstructed by a purely random method.

2.3. Mathematical Model

To establish the model equations, we made the following assumptions.

- Volume change of material during cell operations is not taken into account, i.e., constant porosity in electrodes and separator;
- Charge transfer kinetics follows the Butler-Volmer equation;
- Electrochemical reactions occur at the solid active materials/electrolyte interfaces;
- Interfacial electrical equilibrium exists in both the electrolyte and solid active materials and interfacial chemical equilibrium exists in the electrolyte phase;
- Side reactions do not occur;
- Ionic species transport in the electrolyte is by diffusion and migration, and lithium transport inside the solid active material particles by diffusion;
- The solid and electrolyte phases are immobile during battery operations.

The multi-disciplinary transport processes coupled with electrochemical reactions in lithium-ion battery are then described by a series of conservation equations.

2.3.1. Charge Conservation Equations

The electron charge conservation in solid phases (including additives and active materials) is governed by

$$\nabla \cdot \left(\sigma \nabla \varnothing\right) - j^{Li} = 0 \quad (3)$$

where ϕ_s, σ, and j are the solid phase potential, electronic conductivity of solid phase, and the transfer current density, respectively. Boundary conditions for galvanostatic (with constant current I) discharge/charge are

$$-\sigma \frac{\partial \varnothing_s}{\partial x}\Big|_{x=0} = -\sigma \frac{\partial \varnothing_s}{\partial x}\Big|_{x=X} = \frac{I}{A} \quad (4)$$

where X is the thickness of lithium-ion battery, A is the surface area of current collector. x=0 denotes the position of anode current collector outward surface, x=X the cathode current collector outward surface. For

discharge processes *I* is positive while for charge process *I* is negative. For potentiostatic charge processes, the two outer surfaces are both subject to a constant voltage.

The Li^+ charge conservation in electrolyte phase is described by

$$\nabla\cdot\left(K\nabla\varnothing_e\right)+\nabla\cdot\left(K_D\nabla In\, c_e\right)+j^{Li}=0 \tag{5}$$

where ϕ_e denotes the electrolyte phase potential, the ionic conductivity κ is given by [25]

$$K=4.1253\times10^{-4}+5.007c_e-4.7212\times10^{3}c_e^{\,2}+1.5094\times10^{6}c_e^{\,3}-1.6018\times10^{8}c_e^{\,4} \tag{6}$$

with c_e being the Li^+ concentration in the electrolyte phase. The ionic diffusional conductivity, κ_D, is given by

$$K_D=\frac{2RTK}{F}\left(t_+^{\,0}-1\right)\left[1+\frac{d\mathrm{In}\, f\pm}{d\mathrm{In}c_e}\right] \tag{7}$$

where *F* is the Faraday's constant, *R* the universal gas constant, and *T* the absolute temperature in Kelvin. t_+^0 denotes the transference number of Li^+. Depending on the combination of electrolyte and solvent, the transference number t_+^0 can be a function of Li^+ concentration in electrolyte. The mean molar activity coefficient of the electrolyte $f_\pm$ is assumed constant in the present work. In the two current collectors, there exist only electronic current (ionic current equals zero). Accordingly, we obtain boundary conditions for electrolyte potential as

$$\left.\frac{\partial\varnothing_e}{\partial_x}\right|_{x=0}=\left.\frac{\partial\varnothing_e}{\partial_x}\right|_{x=X}=0 \tag{8}$$

The transfer current density j^{Li} occurring only at the solid active material/electrolyte interface is determined from the Butler-Volmer equation, which describes the reaction flux on the particle surface as a function of the exchange current density i_0 and the surface overpotential η_{int}, as

$$j^{Li}=\frac{A_{lm}}{V}i_0\left[\exp\left[\frac{\alpha_{an}F\eta_{\mathrm{int}}}{RT}\right]-\exp\left[-\frac{\alpha_{ca}F\eta_{\mathrm{int}}}{RT}\right]\right] \tag{9}$$

where *l*, *m* denotes solid active material and electrolyte, respectively. α_{an} and α_{ca} are the anodic and cathodic transfer coefficients of electrode reaction j^{Li}. As A_{lm} is the interfacial area of phase *l* and *m*, and *V* is the total volume of the control unit, the ratio of A_{lm} to *V* is actually the local specific surface area of solid active materials. The exchange current density, i_0, exhibits modest dependency on the Li^+ concentration in electrolyte and Li concentration at the solid active material surface, respectively. That is

$$i_0=kFc_{S,\max}\left(c_e\right)^{\alpha an}\left[\frac{c_S}{c_{S,\max}}\right]^{\alpha ca}\left[1-\frac{c_S}{c_{S,\max}}\right]^{\alpha an} \tag{10}$$

where *k* is the rate constant of the electrochemical reaction. The overpotential η_{int} is associated with the solid active material/electrolyte interface, and is defined as the solid phase potential in the solid active material side ($\phi_{s,l}$) deducted by the electrolyte phase potential in the electrolyte side ($\phi_{e,m}$) and the open-circuit potential (*U*), i.e.

$$\eta^{\mathrm{int}}=\varnothing_{S,l}-\varnothing_{e,m}-U \tag{11}$$

The open-circuit potential *U* is a function of the local state of charge, θ [25], expressed as

$$U_{an}=0.722+0.1387\theta+0.029\sqrt{\theta}-\frac{0.0172}{\theta}+\frac{0.0019}{\theta^{1.5}}+0.2808\exp\left(0.90-15.0\theta\right)-0.7984\exp\left(0.4465\theta-0.4108\right) \tag{12}$$

$$U_{ca}=\frac{-4.65+88.669\theta^2-401.119\theta^4+}{-1.0+18.933\theta^2-79.532\theta^4+}\cdot\frac{342.909\theta^6-462.471\theta^8+433.434\theta^{10}}{37.311\theta^6-73.083\theta^8+95.96\theta^{10}} \tag{13}$$

The local state of charge (SOC) or depth of discharge (DOD), θ, is the Li concentration on the solid active material/electrolyte interface divided by the maximum Li concentration that the solid active materials can accommodate, i.e.

$$\theta=\frac{c_S}{c_{S,\max}} \tag{14}$$

Therefore, compared with the macroscopic models, the mesoscopic pore-scale model more accurately resolves the complex electrochemical reactions, which are prescribed to occur only at the interfaces of solid active materials and electrolyte.

2.3.2. Species Conservation Equations

Diffusion is the major mechanism for transport of Li inside solid active materials. Therefore, the Li species conservation equation in solid active materials (not including the additives) is formulated as the following

$$\frac{\partial c_S}{\partial t} = \nabla \cdot \left(D_S \nabla c_S \right) \tag{15}$$

where c_s and D_s denote the Li concentration in solid active materials and the Li diffusivity, respectively. One boundary condition is

$$-D_s \frac{A_{lm}}{V} \frac{\partial_{cS}}{\partial \mathbf{n}}\Big|_{\Omega} = \frac{j^{Li}(t)}{F} \tag{16}$$

where ***n*** denotes the external normal direction of solid active materials, Ω represents the interface of solid active material particles and electrolyte. Inside the two current collectors there is no flux of Li species, one more boundary condition for Li species transport thus yields as

$$\frac{\partial c_S}{\partial x}\Big|_{x=0} = \frac{\partial c_S}{\partial x}\Big|_{x=X} = 0 \tag{17}$$

The Li^+ species conservation equation in electrolyte phase is formulated as the following

$$\frac{\partial c_e}{\partial t} = \nabla \cdot \left(D_e \nabla c_e \right) + \frac{1 - t_+^{\,0}}{F} j^{Li} - \frac{\mathbf{i}_e \cdot \nabla t_+^{\,0}}{F} \tag{18}$$

where c_e denotes the Li^+ concentration in the electrolyte phase, $\mathbf{i}_e$ is the current density vector, and D_e the mass diffusion coefficient of Li^+ in the electrolyte. In this work, a constant value of the transference number of Li^+ is assumed [9], and thus the last term on the right hand side of Eq. (18) is omitted. Inside the two current collectors, the flux density of Li^+ species must be zero. Therefore, we obtain the boundary conditions for Li^+ species transport as

$$\frac{\partial c_e}{\partial x}\Big|_{x=0} = \frac{\partial c_e}{\partial x}\Big|_{x=X} = 0 \tag{19}$$

2.3.3. Energy Conservation Equation

The energy conservation equation is formulated as

$$\rho C_P \frac{\partial T}{\partial t} = \nabla \cdot \left(\lambda \nabla T \right) + Q \tag{20}$$

where T, λ, and ρC_p denote the temperature, heat conductivity, and volumetric heat capacity, respectively; the heat generation rate Q is expressed as [9]

$$\begin{aligned} Q = {} & j^{\mathrm{Li}} \left[\varnothing_S - \varnothing_e - U + T \frac{\partial U}{\partial T} \right] + \\ & \left(K_D \nabla \ln c_e \nabla \varnothing_e + K \nabla \varnothing_e \nabla \varnothing_e \right) + \sigma \nabla \varnothing_S \nabla \varnothing_S + Q_c \end{aligned} \tag{21}$$

The first term on the right hand side of Eq. (21) represents the electrochemical reaction heat, the second and third term come from the joule heating in the electrolyte and solid phases, respectively, and the last term represents the heat generation due to contact resistance and the resistance of SEI film. We consider only convective heat release to the environment and write the thermal boundary conditions as

$$-\lambda \frac{\partial T}{\partial x}\Big|_{x=0} = -\lambda \frac{\partial T}{\partial x}\Big|_{x=X} = h_E \left(T - T_E \right) \tag{22}$$

where h_E denotes the convective heat transfer coefficient and T_E the temperature of environment.

In the above equations, all the physicochemical properties are location-dependent and component-wise. For example, the species transport of Li^+ only occurs in the electrolyte, thus the component-wise Li^+ diffusivity field is defined as

$$D_e = \begin{cases} D_{e,0}\left(c_e, T \right) & \textit{In electrolytephase} \\ 0 & \textit{In solid phase and current collector} \end{cases} \tag{23}$$

where $D_{e,0}$ is the inherent diffusivity of the location component.

2.3.4. Thermal and Electrochemical Coupling

To accommodate the thermal and electrochemical coupling effects, temperature- dependent physico-chemical properties are considered and the temperature-dependence is described by the Arrhenius' equation [26]

$$\Phi = \Phi_{ref} \exp\left[\frac{E_{act,\Phi}}{R} \left[\frac{1}{T_{ref}} - \frac{1}{T} \right] \right] \tag{24}$$

where Φ is a general variable representing κ, D_s, D_e, etc., Φ_{ref} is the value at a reference temperature T_{ref}, and $E_{act,\Phi}$ the activation energy of the evolution process of Φ, the magnitude of which indicates the sensitivity of Φ to temperature.

2.4. Numerical Strategy

All the governing equations of the primary variables, i.e. Eqs. (3), (5), (15), (18) and (20), can be described in the following general form

$$\frac{\partial \Phi}{\partial t} = \nabla \left(\Gamma \nabla \Phi \right) S_\Phi \tag{25}$$

where Φ denotes a general-purpose variable (i.e., concentration, potential or temperature), Γ is the diffusion coefficient, and S_Φ is the source term that includes all the terms that cannot be included in the previous terms.

The governing equations are discretized and solved by a commercial CFD flow software, such as Fluent®, or by self-developed solvers, such as the smoothed particle hydrodynamic (SPH) solver developed in [27]. The present work takes the Fluent® solver, which is based on the finite volume (FV) approximation. By customizing its User Defined Functions (UDF), various source terms and physicochemical properties are implemented. The first order upwind differencing scheme is generally used to discretize the spatial-derivative terms and a fully implicit scheme is used to discretize the transient terms. To accelerate convergence, the algebraic multi-grid (AMG) iterative method is applied to solve the linearized algebraic equations.

3. RESULTS AND DISCUSSION

For the test case, the thicknesses of the anode current collector, anode electrode, separator, cathode

Table 1: Geometrical And Operating Conditions

Thickness-x(μm)					Periodic boundry in y and z	
Anode CC	**Anode Electrode**	**Seprator**	**Cathode Electrode**	**Cathode CC**	**y-height(μm)**	**z-height**
4	40	25	35	8	10	10

Operating conditions (discharge)						
Initial SOC		**Discharge current (A/m^2)**	**Initial temperature (K)**	**Heat convection coefficient ($W/m^2/K$)**	**Teperature of environment (K)**	**Initial C_e (mol/m^3)**
Anode	**Cathode**					
0.89	0.51	10.15(Case 1: 1C; Case 2: 0.675C	298.15	20.0	298.15	1000.0

Table 2: Physicochemical Properties

	Cu	**Li_xC_6**	**CMC+SBR etc.**	**Electrolyte**	**Polymer**	**SP+PVDF etc.**	**$Li_{y-x}CoO_2$**	**Al**
λ ($W\ m^{-1}\ K^{-1}$)	380	0.1	0.5	0.01	0.05	0.5	0.1	200
ρC_p ($W\ m^{-3}\ K^{-1}$)	3.4×10^6	2.5×10^6	3.0×10^6	0.6×10^6	1.5×10^6	3.0×10^6	2.0×10^6	2.4×10^6
σ ($S\ m^{-1}$)	6.0×10^7	2.0	20.0	0	0	20.0	0.1	3.8×10^7
κ ($S\ m^{-1}$)	0			Eq. (6)	0			
κ_D ($A\ m^{-1}$)	0			Eq. (7)	0			
D_s ($m^2\ s^{-1}$)	0	3.9×10^{-14}	0				1.0×10^{-13}	0
D_e ($m^2\ s^{-1}$)	0			7.5×10^{-11}	0			
$c_{s,max}$ ($mol\ m^{-3}$)	N/A	28688.8	N/A				53147.5	N/A
$c_{e,0}$ ($mol\ m^{-3}$)	N/A			1000.0	N/A			

k_{an}, k_{ca} ($m^{2.5}\ mol^{-0.5}\ s^{-1}$)	1.764×10^{-11}, 6.667×10^{-11}
α_{an}, α_{ca}	0.5, 0.5
U_{an}, U_{ca} (V)	Eq. (12), Eq. (13)
t_+^0	0.363
$E_{act,\ De}$ ($J\ mol^{-1}$)	4000
$E_{act,\ Ds,an}$, $E_{act,\ Ds,ca}$ ($J\ mol^{-1}$)	4000, 20000
$E_{act,\ \kappa}$ ($J\ mol^{-1}$)	4000

electrode, and cathode current collector are 4, 40, 25, 35, and 8μm, respectively; in the directions (i.e. y and z) perpendicular to the battery thickness direction (i.e. x), we assume periodic boundary conditions so that many repeating 10×10 μm units constitute a battery of practical size. We only simulate discharge processes in this particular work. (For charge processes, the solution procedure is the same though the cell may have different solid phase potential boundary conditions and is in a different initial state.) The cell is discharging at a a current density, 10.15 A/m^2, i.e., at the rate of 1C. Geometrical and operating conditions are tabulated in Table **1**. Important physicochemical properties implemented in the simulations are summarized in Table **2**. Some parameters listed in Table **2** are taken from Refs. [9] and [25]. Geometrical design and operating parameters listed in Table **1** and the remaining physicochemical parameters in Table **2** are from our industrial partner, Amperex Technology Limited (ATL-Dongguan), except the parameters, $c_{s,max}$-s, which are calculated from the chemical formulae of anode and cathode active materials.

The simulation results give detailed distributive information of all the primary and participating variables related to the involved multidisciplinary process in the battery during discharge. Figures **3-5** exemplify the obtained results of Li^+ concentration in electrolyte phase, Li concentration in solid active materials, electrolyte phase potential, and solid phase potential. We show the calculated 3D distribution at two representative time instants, 8.0 s and 1201.3 s, and the derived profile of cross-sectional averages along the thickness direction for each variable.

During discharge, the anode electrochemical reaction produces Li^+, which are dissolved in the electrolyte and transported to the cathode; the cathode consumes Li^+ in the electrolyte and turns them into Li

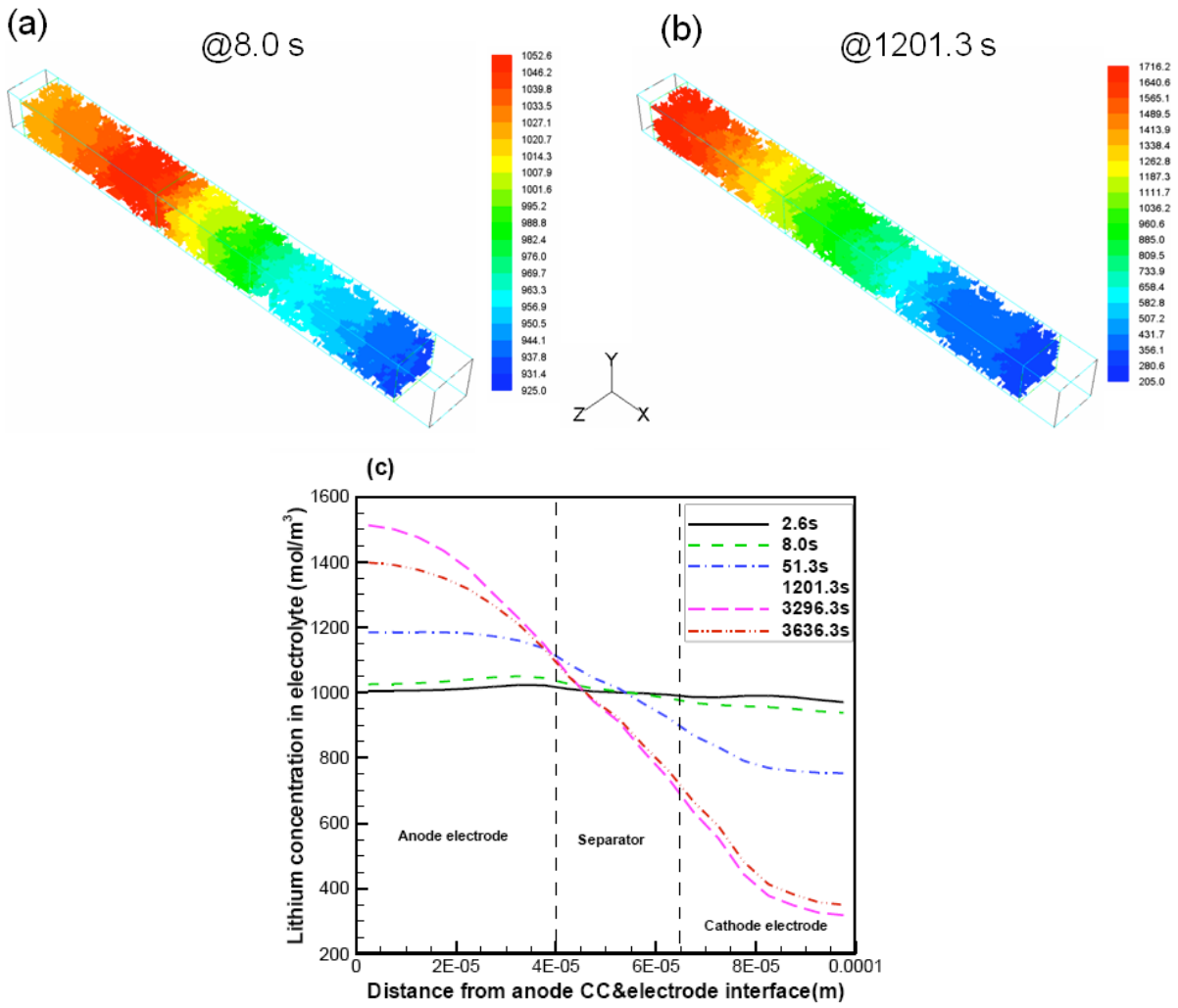

Figure 3: Li^+ concentration (mol/m^3) in electrolyte phase during discharge. 3D distributions at two representative time instants, 8.0s (**a**) and 1201.3s (**b**); Profile of cross-sectional averaged Li^+ concentration in electrolyte phase and its temporal evolution (**c**).

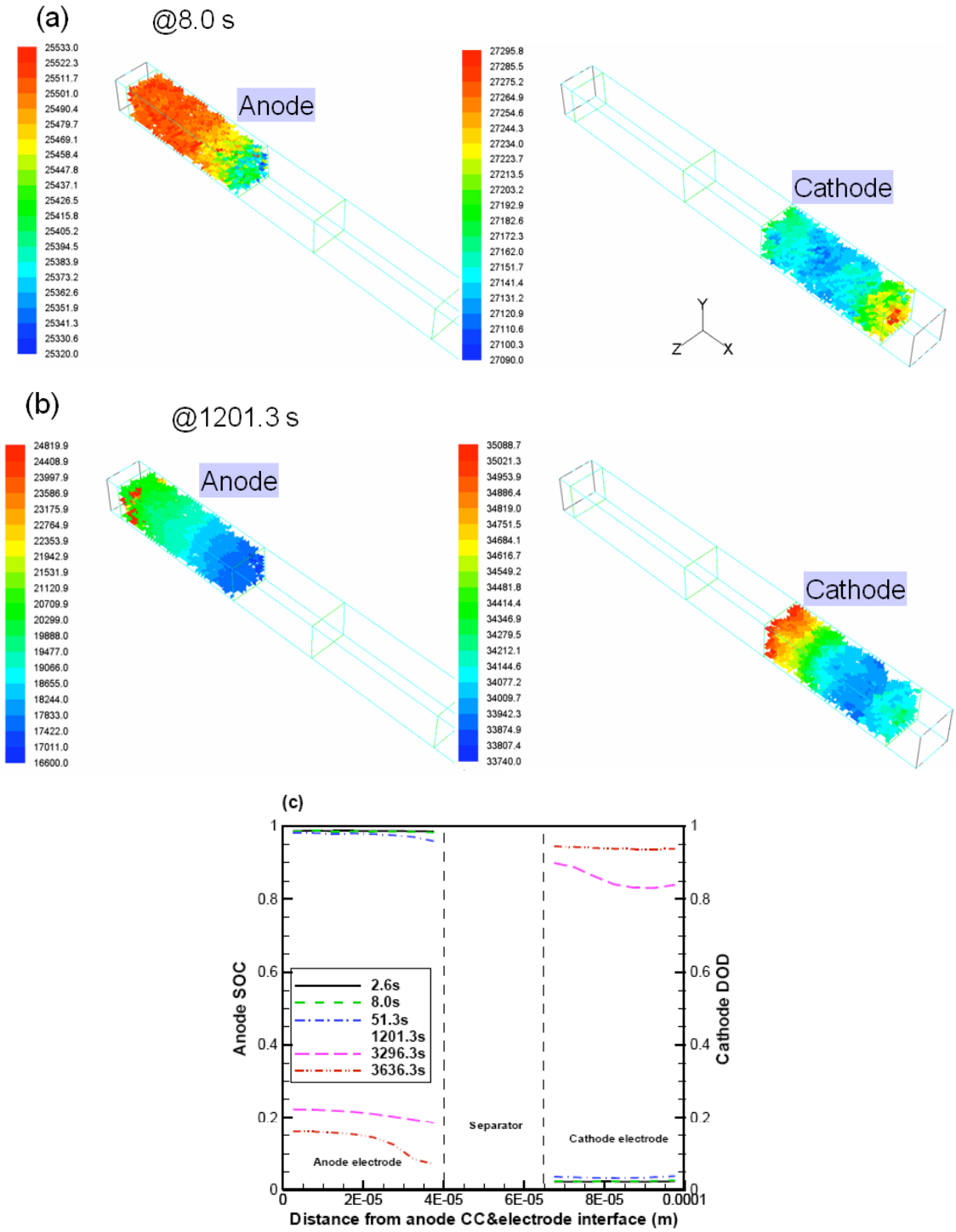

Figure 4: Li concentration (mol/m^3) in solid active materials during discharge. 3D distributions at two representative time instants, 8.0s (**a**) and 1201.3s (**b**); Profile of cross-sectional averaged SOC or DOD and its temporal evolution (**c**).

atoms to insert into the active material particles. Seen from the results of Li^+ concentration in electrolyte phase shown in Figure **3**, an evident Li^+ concentration Gradient is gradually forming in the electrolyte phase, which drives the Li^+ to transport from anode to cathode.

In Figure **4** are displayed the results about Li concentration distribution in solid active materials. The Li concentration continuously decreases in the anode electrode and increases in the cathode electrode with the progress of discharge process. The anode electrochemical reaction consumes Li atoms at the surfaces of anode active material particles and produce Li^+, which dissolve and transport in the electrolyte, penetrate the separator, and finally reach the cathode.

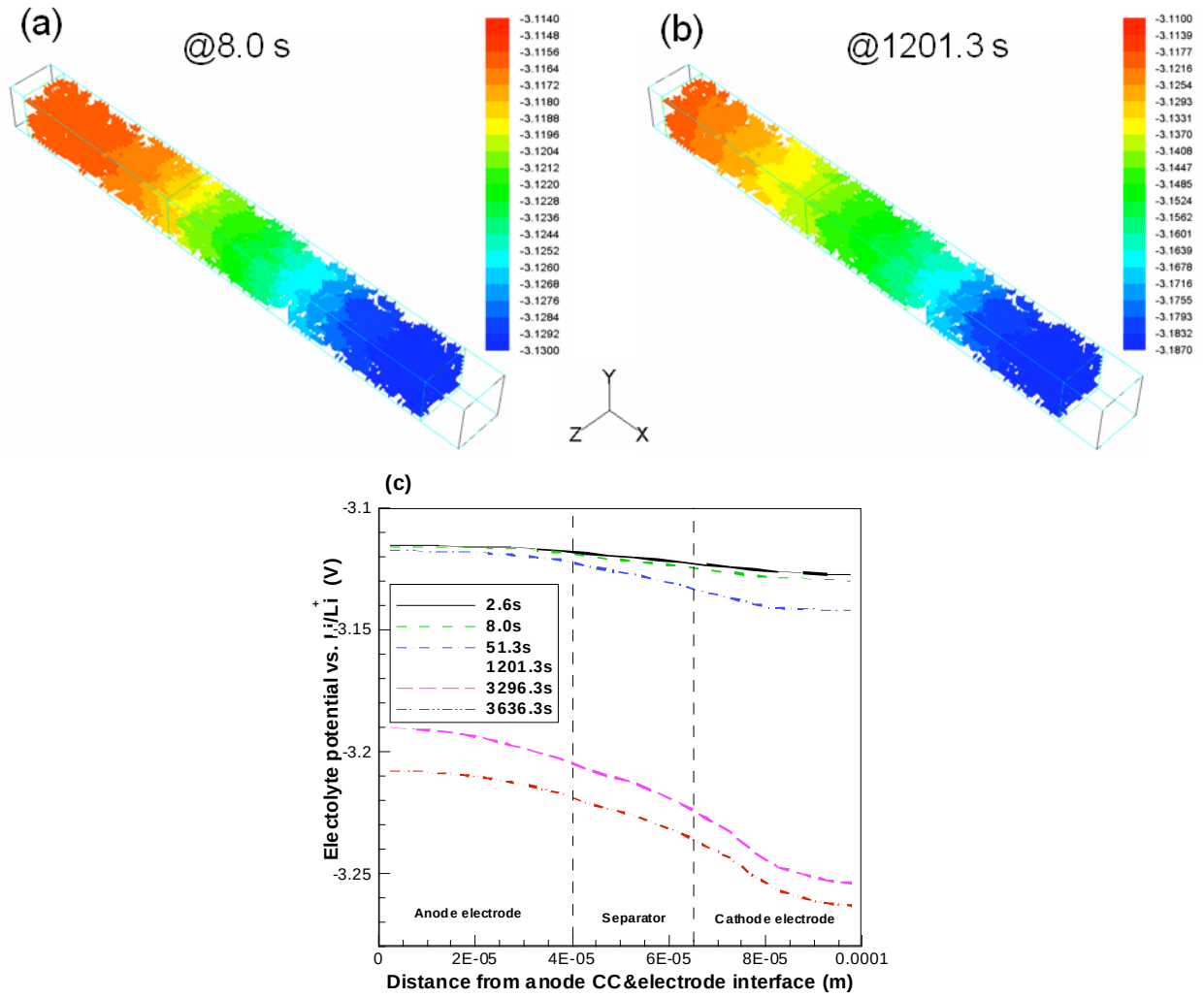

Figure 5: Electrolyte phase potential (V, versus Li/Li^+) during discharge. 3D distributions at two representative time instants, 8.0s (**a**) and 1201.3s (**b**); Profile of cross-sectional averaged electrolyte phase potential and its temporal evolution (**c**).

The cathode electrochemical reaction changes the Li^+ in the electrolyte at the active material particle/electrolyte interfaces into Li atoms, which insert into the active material particles. In both the anode and cathode, the Li concentration in solid active materials at a same time instant is not uniformly distributed and the Li concentrations at different positions do not evolve synchronously, indicating uneven electrochemical reactions occurring inside the cell.

During discharge process, charge transport of Li^+ needs a distribution of phase potential to be established in the electrolyte phase. Figure **5** shows the calculated results of electrolyte phase potential distribution. The electrolyte phase potential decreases along the battery thickness direction, indicating Li^+ charge transport from the anode electrode to the cathode electrode. The electrolyte phase potential is diminishing with the discharge time due to the decrease of SOC or increase of DOD.

During discharge process, electrons produced in the anode electrode are transported to the cathode electrode by passing the external circuit. Inside the battery, a solid phase potential distribution will be established to support the flow of electrons. Figure **6** presents the calculated results of solid phase potential. In the anode, the solid phase potential decreases towards the separator side, which drives the electrons to flow from the anode electrode to the current collector. In the cathode, the solid phase potential increases towards the separator side, meaning the electrons are flowing from the cathode current collector to the electrode. The solid phase potential drop in the anode is much smaller than that in the cathode owing to the much smaller electron transport resistance in the anode. As the reference potential (-3.02V) is set in the anode current collector, the magnitude of solid phase potential in the anode is almost unchanged throughout the discharge process. However, in the cathode the

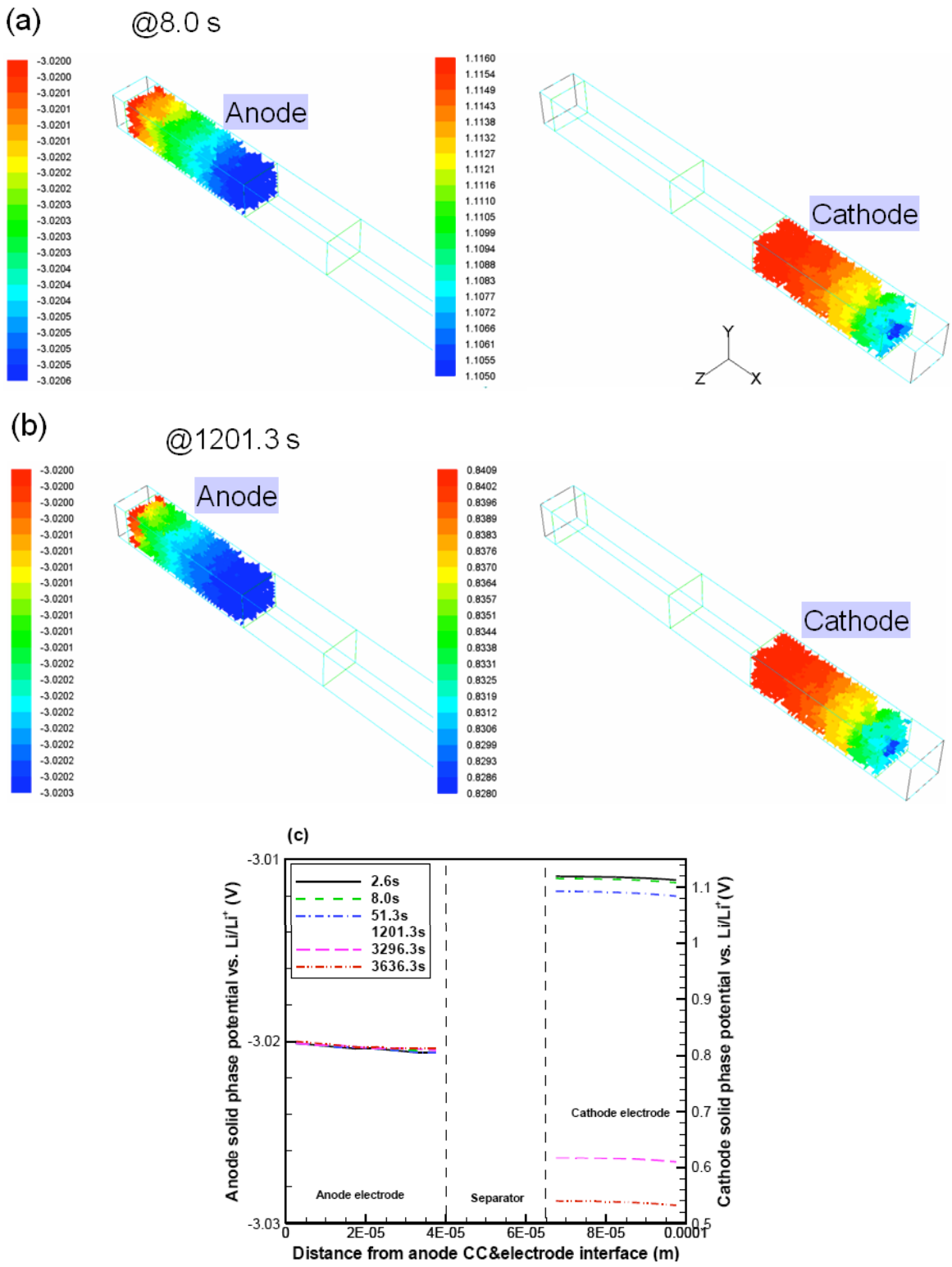

Figure 6: Solid phase potential (V, versus Li/Li^+) during discharge. 3D distributions at two representative time instants, 8.0s (**a**) and 1201.3s (**b**); Profile of cross-sectional averaged solid phase potential and its temporal evolution (**c**).

solid phase potential is decreasing with the discharge process due to the decrease of SOC.

The output cell voltage is the solid phase potential at the outward surface of the cathode current collector deducted by that of the anode current collector. The calculated cell voltage as a function of discharge time is displayed in Figure **7**. The cell voltage continuously decreases with the discharge time. If the cut-off voltage is set at 3.2 V, the discharge duration is about 3656 s,

meaning the discharge process can fully discharge the total energy stored in the cell and no evident transport limiting presents.

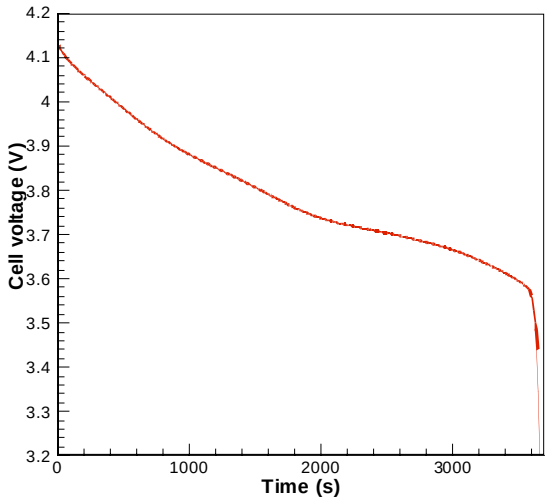

Figure 7: Calculated cell voltage evolution during discharge.

The calculated typical temperature distribution inside the cell is displayed in Figure **8**. We see very small temperature rise and almost uniform temperature distribution inside the cell, meaning the heat generation during discharge can be released to the ambient in time. This is due to the thin electrodes and the imposed relatively strong convective heat release (heat convective coefficient =20 W m^{-2} K^{-1}) at the outer surfaces of the current collectors.

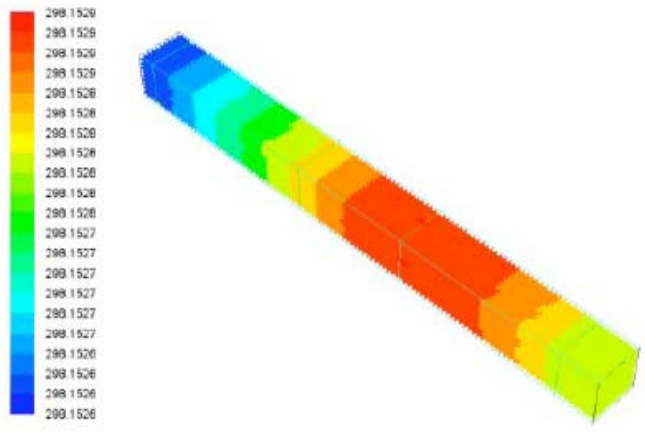

Figure 8: Calculated typical temperature (K) distribution in the cell during discharge.

4. SUMMARY AND OUTLOOK

We developed a 3-dimensional DNS model for Li-ion battery charge/discharge processes. This model employs the FV numerical technique and solves component-wise multidisciplinary transport equations based on a mesoscopic resolution of electrode microstructures. We then performed one test case, in which the electrode microstructures were reconstructed by a purely random method. Results indicated that this model is not only able to predict macroscopic parameters such as the output cell voltage, but also capable of giving detailed distribution information of all the primary and participating variables, including solid/electrolyte phase potential, Li^+ concentration in electrolyte, Li concentration in solid active materials, and transfer current density at the solid active materials/electrolyte interfaces, etc. The validity of the model was thus corroborated.

As the developed DNS model is based on microstructure of composite electrodes and solves component-wise transport equations, it has unique advantages over macroscopic models, e.g., i) the input physical properties are intrinsic material properties, not effective physical properties in macroscopic models; ii) the electrochemical reactions are prescribed to occur exactly on the interface of solid and electrolyte phase. Therefore, the DNS model has the potential to unravel the underlying mesoscopic pore-scale mechanisms of multi-disciplinary transport coupled with electro-chemical reactions and thus can provide more insightful information of the involved processes, as well as enables the design and optimization of electrodes, including microstructures inside electrodes. Future work will deal with model validation/calibration by carrying out more simulations including simulations to charge processes and conducting necessary experiments, further the model development such as the development of more advanced electrode microstructure reconstruction approach, and utilize the model for the design/optimization of electrodes.

ACKNOWLEDGEMENTS

Financial support received from the China National Natural Science Foundation (51206171), Amperex Technology Limited (ATL-Dongguan), and CAS “100 talents” Plan (FJ) is gratefully acknowledged.

REFERENCES

[1] Scrosati B, Garche J. Lithium batteries: status. prospects and future. J Power Sources 2010; 195: 419-2430. http://dx.doi.org/10.1016/j.jpowsour.2009.11.048

[2] Bandhauer TM, Garimella S, Fuller TF. A critical review of thermal issues in lithium-ion batteries. J Electrochem Soc 2011; 158: R1-R25. http://dx.doi.org/10.1149/1.3515880

[3] West K, Jacobsen T, Atlung S. Modeling of porous insertion electrodes with liquid electrolyte. J Electrochem Soc 1982; 129: 1480-1485. http://dx.doi.org/10.1149/1.2124188

[4] Doyle M, Fuller TF, Newman J. Modeling of galvanostatic charge and discharge of lithium/ polymer/insertion cell. J Electrochem Soc 1993; 140: 1526-1533. http://dx.doi.org/10.1149/1.2221597

[5] Pals CR, Newman J. Thermal modeling of the lithium/polymer battery I. Discharge behavior of a single cell. J Electrochem Soc 1995; 142: 3274-3281. http://dx.doi.org/10.1149/1.2049974

[6] Pals CR, Newman J. Thermal modeling of the lithium/polymer battery II. Temperature profiles in a cell stack. J Electrochem Soc 1995; 142: 3282-3288. http://dx.doi.org/10.1149/1.2049975

[7] Chen Y, Evans JW. Heat transfer phenomena in lithium/ polymer-electrolyte batteries for electric vehicle application. J Electrochem Soc 1993; 140: 1833-1838. http://dx.doi.org/10.1149/1.2220724

[8] Chen Y, Evans JW. Three-dimensional thermal modeling of lithium-polymer batteries under galvanostatic discharge and dynamic power profile. J Electrochem Soc 1994; 141: 2947-2955. http://dx.doi.org/10.1149/1.2059263

[9] Gu WB, Wang CY. Thermal-electrochemical modeling of battery systems. J Electrochem Soc 2000; 147: 2910-2922. http://dx.doi.org/10.1149/1.1393625

[10] Srinivasan V, Wang CY. Analysis of electrochemical and thermal behavior of lithium-ion cells. J Electrochem Soc 2003; 150: A98-A106. http://dx.doi.org/10.1149/1.1526512

[11] Jiang FM, Peng P, Sun YQ. Thermal analyses of $LiFePO_4$/graphite battery discharge processes. J Power Sources 2013; 243: 181-194. http://dx.doi.org/10.1016/j.jpowsour.2013.05.089

[12] Jiang FM, Zeng JB, Wu W. Design and optimization of lithium-ion battery electrodes: mesoscopic pore-scale numerical model. Advanced Materials Industry 2011; 12: 2-6. (in Chinese)

[13] Orszag SA. Analytical theories of turbulence. J Fluid Mechanics 1970; 41: 363-386. http://dx.doi.org/10.1017/S0022112070000642

[14] Baritaud T, Poinsot T, Baum M. Direct numerical simulation for turbulent reacting flows. Paris, Editions Technip 1996.

[15] Wang GQ, Mukherjee PP, Wang CY. Direct numerical simulation (DNS) modeling of PEFC electrodes Part I. Regular microstructure. Electrochim Acta 2006; 51: 3139-3150. http://dx.doi.org/10.1016/j.electacta.2005.09.002

[16] Wang GQ, Mukherjee PP, Wang CY. Direct numerical simulation (DNS) modeling of PEFC electrodes Part II. Random microstructure. Electrochimica Acta 2006; 51: 3151-3160. http://dx.doi.org/10.1016/j.electacta.2005.09.003

[17] Mukherjee PP, Wang CY. Stochastic microstructure reconstruction and direct numerical simulation of the PEFC catalyst layer. J Electrochem Soc 2006; 153: A840-A849. http://dx.doi.org/10.1149/1.2179303

[18] Mukherjee PP, Wang CY. Direct numerical simulation modeling of bilayer cathode catalyst layers in polymer electrolyte fuel cells. J Electrochem Soc 2007; 154: B1121-B1131. http://dx.doi.org/10.1149/1.2776221

[19] Zhang X, Sastry AM, Shyy W. Intercalation-induced stress and heat generation within single lithium-ion battery cathode particles. J Electrochem Soc 2008; 155: A542-A552. http://dx.doi.org/10.1149/1.2926617

[20] Wang CW, Sastry AM. Mesoscale modeling of a Li-ion polymer cell. J Electrochem Soc 2007; 154: A1035-A1047.

[21] Garcia RE, Chiang YM, Carter WC, Limthongkul P, Bishop CM. Microstructural modeling and design of rechargeable lithium-ion batteries. J Electrochem Soc 2005; 152: A255-A263.

[22] Garcia RE, Chiang YM. Spatially resolved modeling of microstructurally complex battery architectures. J Electrochem Soc 2007; 154: A856-864.

[23] Smith M, Garcia RE, Horn QC. The effect of microstructure on the galvanostatic discharge of graphite anode electrodes in $LiCoO_2$-based rocking-chair rechargeable batteries. J Electrochem Soc 2009; 156: A896-A904.

[24] Awarke A, Wittler M, Pischinger S, Bockstette J. A 3D mesoscale model of the collector-electrode interface in Li-Ion batteries. J Electrochem Soc 2012; 159: A798-A808.

[25] Ramadass P, Haran B, Gomadam PM, White R, Popov BN. Development of first principles capacity fade model for Li-ion cells. J Electrochem Soc 2004; 151: A196-A203.

[26] Kuzminskii YV, Nyrkova L, Andriiko AA. Heat generation of electrochemical systems batteries. J Power Sources 1993; 46: 29-38. http://dx.doi.org/10.1016/0378-7753(93)80032-K

[27] Zeng JB, Jiang FM, Chen Z. A pore-scale smoothed particle hydrodynamics model for lithium-ion batteries. Chin Sci Bull 2014; 59: 2793-2810. http://dx.doi.org/10.1007/s11434-014-0354-y

Received on 05-11-2014 Accepted on 16-11-2014 Published on 09-01-2015

DOI: http://dx.doi.org/10.15377/2409-5826.2014.01.02.1